Electrical properties of $(Ba,Sr)TiO_3$ thin films revisited: The case of chemical vapor deposited films on Pt electrodes

Peter Ehrhart[a] and Reji Thomas
Institute für Festkörperforschung (IFF) and Center of Nanoelectronic Systems for Information Technology (CNI), Forschungszentrum Jülich, D52428 Jülich, Germany

(Received 20 October 2005; accepted 12 March 2006; published online 9 June 2006)

Due to the dependence on both bulk and interface properties neither the effective dielectric constant ε nor the leakage current J can be scaled in a straightforward manner with film thickness for high-ε thin film capacitors. Based on detailed investigations of different thickness series of $(Ba,Sr)TiO_3$ films on platinized substrates the bulk and interfacial properties are separated. An approach to estimate the apparent interfacial layer thickness is discussed. The behavior of the leakage current is divided in two regions: for low voltages, $\leqslant 1$ V, the currents are very low, $\leqslant 10^{-10}$ A/cm^2, and dominated by the relaxation currents (Curie–von Schweidler behavior). At higher voltages the change to a very strong power law dependence is observed, $J \sim E^{16}$. The thickness dependence is removed by scaling with the internal field or dielectric displacement of the film, $D=\varepsilon_0 \varepsilon E$. Hence, a direct connection between the increase in ε and the increase in leakage with film thickness is revealed. This behavior is accompanied by a larger scatter of the data and seems to be controlled by a more inhomogeneous or local conductivity. Influences of the measuring temperature and of stoichiometry and interfacial properties are discussed. © *2006 American Institute of Physics*. [DOI: 10.1063/1.2202115]

I. INTRODUCTION

High dielectric constant perovskite thin films such as the $Ba_xSr_{1-x}TiO_3$ (BST) solid solution series have been proposed for a very broad application area, including capacitor dielectrics for future dynamic random access memories (DRAMs), embedded capacitors, and tunable devices.[1,2] Pt is considered as a standard metal electrode as it is stable against oxidation at the deposition temperatures and as its high work function helps to reduce leakage currents through the capacitor stack. In spite of intensive research over the last two decades, which has been reviewed recently,[2–7] many details on the structure property relations are not understood in detail. A special problem of the high-ε perovskites is the poor scalability of the capacitance with film thickness, which has been explained phenomenological by an interfacial layer of low capacity, the "dead layer." More recently it has been recognized that the understanding of this dead layer is also important for the understanding of the leakage currents.[8–11]

In a two-capacitor model the contributions of interfacial layers, ε_i, and film, ε_B, can be separated for thickness series of thin films. This model assumes a bulk region of thickness t and permittivity ε_B, and the two interface regions with thickness t_i, which yield two capacitors of a lower permittivity ε_i. Considering the two electrodes as identical the resulting reciprocal capacitance of the film is given by Eq. (1) and the slope of a plot of $1/C$ versus thickness yields the bulk permittivity, and the intercept represents the interface capacitance,

$$\frac{A}{C} = \frac{A}{C_{i1}} + \frac{A}{C_B} + \frac{A}{C_{i2}} \approx \frac{2A}{C_i} + \frac{A}{C_B} = \frac{2t_i}{\varepsilon_0 \varepsilon_i} + \frac{t-2t_i}{\varepsilon_0 \varepsilon_B} \approx \frac{2t_i}{\varepsilon_0 \varepsilon_i} + \frac{t}{\varepsilon_0 \varepsilon_B}. \quad (1)$$

In this approximation the properties of the two interfaces cannot be separated, although they might be different even in the case of identical materials, due to the different growth conditions of bottom and top electrodes. Hence, interfacial properties are characterized in the literature sometimes by t_i/ε_i, for a single average interface, or by $2t_i/\varepsilon_i$, for the total interfacial contribution. This interfacial capacity may conveniently be expressed by the thickness of a SiO_2 dielectric, which yields the same capacity, the equivalent (Si)-oxide thickness, EOT,

$$\mathrm{EOT} = 3.9t/\varepsilon = 3.9\varepsilon_0 A/C. \quad (2)$$

Hence, the total interfacial capacity is $\mathrm{EOT}_i = 3.9\ (2t_i/\varepsilon_i)$. The approximation seems limited, as no straight line is observed over larger thickness ranges in some cases;[11,12] typical data ranges are 20–80 nm, but larger deviations are frequently observed at larger t. At smaller t the assumption, $t_i \ll t$, breaks down and larger experimental uncertainties have to be considered additionally. Hence, the actual thickness range also contributes to the scatter of the published data. Best values observed for the bulk dielectric constant reach values of $\varepsilon_B = 800-1000$ for BST(70/30) and values for the interfacial capacity reach values of $\mathrm{EOT}_i = 0.16-0.3$ nm. Much better values have been reported for epitaxial full oxide capacitor stacks, e.g., $\varepsilon_B = 6600$ and $\mathrm{EOT}_i = 0.03$ nm for $SrRuO_3/BST/SrRuO_3$ capacitors.[13] The interfacial capacity is of course the limiting value for the total capacitor for vanishing layer thickness. No specific

[a]Electronic mail: p.ehrhart@fz-juelich.de

dependencies on deposition techniques, metal organic chemical vapor deposition (MOCVD), sputter deposition, or pulsed laser deposition, have been observed within the limitations given; however, dependencies on film stoichiometry and microstructure have been discussed.

Leakage currents have been less systematically studied, and besides of the dependence on the electrode type, a deduction of systematic trends from data from different sources seems not possible due to the recently realized strong unconventional thickness dependence of the leakage behavior for sputter deposited[14] as well as for MOCVD films.[15] The presence of a dead layer is an important aspect in the understanding of this behavior as it yields an inhomogeneous distribution of the electric field: a large drop within the low-ε interfacial layer and a smaller one within the high-ε film.[8,10] Most of the models for the leakage current concur that the Pt/BST interface forms a Schottky barrier whose barrier height is an important parameter. Nevertheless, the details on the dominating mechanism are under discussion: thermionic emission, field emission, tunneling, as well as the drift diffusion in the bulk.[9,16] All mechanisms can explain certain aspects, however, there is no quantitative description of the effect and its temperature dependence. Hence, inhomogeneous current distributions connected with extended defects (filament formation) should be considered, too. Such effects are well known for different oxides[17] and the local conductivities have been discussed recently for perovskites[18] and especially for $SrTiO_3$.[19]

Hence, a consistent investigation of the dependence of the electrical properties on film stoichiometry, microstructure, and thickness under identical conditions seemed necessary for revealing some generally valid trends as well as their limitations. We have reported on the structural film properties previously,[20] and concentrate on the electrical properties here. As the best and most reproducible data were obtained for films deposited at temperatures $\geqslant 600\ ^\circ C$, we selected such films, although lower temperatures seem necessary for technological applications in order to achieve good conformal deposition on small structures[21,22] and to avoid degradation of the contact plugs.[3] As the results indicate a different stoichiometry dependence of the electrical properties of film and interface, we have additionally modulated the stoichiometry of the interface in order to test the options for an optimization of the electrical properties of the capacitor stacks.

II. EXPERIMENTAL DETAILS

The BST films were deposited by MOCVD in an AIXTRON 2600G3 Planetary Reactor® on platinized silicon wafers. Deposition temperatures were measured at the susceptor and the actual temperature of the wafer surface may be 20–50 °C lower. We discuss films deposited at $595\ ^\circ C < T < 655\ ^\circ C$ and as there was no significant difference observed, we will refer to a deposition temperature of 600 °C. (100)-textured films were observed on Pt(111) electrodes for all film compositions. Details on deposition and structural characterization have been reported previously.[20]

For electrical measurements, Pt electrodes (~100 nm thick) were sputter deposited on top of the BST films and patterned using shadow masks or lift-off lithography. Pad sizes of 1.0, 0.20, 0.05, 0.018, and 0.008 mm^2 were produced. A post-electrode-deposition annealing was performed at 550 °C in artificial air for 20 min in order to remove the sputter damage.[23,24] As this temperature is lower than the deposition temperatures (595–655 °C) the obtained data correspond to the as-deposited films. Only small improvement ($\leqslant 10\%$ in ε_{eff}) has been observed after postdeposition annealing at 750 °C in contrast to the observations with low temperature (400–480 °C) deposited films.[25–27] The polarity of the bias voltages given in this report refers to the voltage difference of the top electrode relative to that of the bottom electrode. Capacitance-voltage (*C-V*) curves and loss tangents were measured with an HP No. 4284 *LCR* meter using a frequency of 100 kHz. Leakage currents were measured using a Burster 4462 voltage generator and a Keithley 617 electrometer with a detection limit of 50 fA. Current-voltage (*I-V*) curves were generated by a stepwise increase of the voltage and the current data were taken after a holding time of 100 s after the voltage steps. The short time relaxation currents were investigated with an aixACCT TF-2000 analyzer in connection with a relaxation module. This module used a fast linear amplifier for the time scale of microseconds and switched to a logarithmic amplifier for larger times. Standard characterization was performed at room temperature (RT).

III. DIELECTRIC PROPERTIES OF STO AND BST FILMS

A. Homogeneous films

The dielectric behavior was characterized by *C-V* curves and the results of the zero bias capacitance measured at RT are summarized in Figs. 1 and 2 in terms of the reciprocal capacitance, or EOT, for $SrTiO_3$ (STO) films and $(Ba_{0.7}Sr_{0.3})TiO_3$ films, respectively. Films with different stoichiometry and a typical thickness range from 15 to 150 nm are compared. For STO there is no dependence on the film stoichiometry, Gr-II/Ti ratio, observed within the given range of deviations from the ideal stoichiometry. In contrast, for $(Ba_{0.7}Sr_{0.3})TiO_3$ films, there is a significant change for Gr-II/Ti > 1, as shown in Figs. 2(a)–2(c). For all cases the data can be reasonably well represented by a straight line and Table I summarizes the corresponding results for the bulk permittivity and the interfacial capacitance. There are rather large uncertainties of the extrapolated values, especially for smaller thickness ranges, and the exact slope depends on the upper limit of the range of thickness values used.[15,28,29] In spite of these uncertainties we observe a clear indication of a stoichiometry dependency (Gr-II/Ti ratio) for the BST films, a decrease of the interfacial capacitance and an increase of the bulk permittivity with increasing Ti content of the films. This different behavior of bulk permittivity and interfacial layers implies a complex behavior of the measured effective permittivity of the films: for thick films, where the bulk permittivity dominates, the effective permittivity reaches a maximum for stoichiometric films as discussed in Ref. 2 for

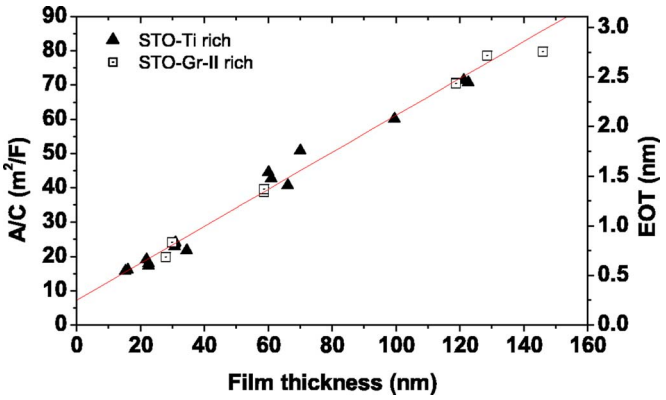

FIG. 1. Thickness dependence of the reciprocal capacitance for STO films with different Gr-II/Ti ratio.

the case of ~60 nm thick films; for thin films of 20–30 nm, which are most relevant for DRAM applications, the interface becomes more important and we observe a saturation or slight increase of the effective permittivity for Gr-II/Ti>1. This tendency cannot be observed for the STO films. The values of $\varepsilon_i/2t_i$ for the STO films are always at the upper limit of the values obtained for $(Ba_{0.7}Sr_{0.3})TiO_3$. As the nucleation and growth behavior for both types of films is very similar this difference indicates that the incorporation of the Ba atoms might be responsible for the changes in the interfacial properties. This behavior might offer possibilities for further optimization of the film stack by changing the chemistry between the nucleation layer and the bulk.

In addition, the table contains the best effective values of the capacity obtained for the different types of films, which is typically obtained for the thinnest films; for STO this value is a factor of 2 lower than the limiting value of the interfacial capacity. For BST the slope of the curve is much smaller and within the scatter of the data, the limiting value of the average line is nearly attained for best films, i.e., the final value is determined by the interfacial capacitance.

There is generally quite good agreement with published values of the dielectric constant (DK) of as-deposited films,[3,11,12,25,30–33] however, a detailed comparison is reasonable only for larger thickness series. In addition, the limited range of the linear $1/C$ behavior, which has been observed by different groups, corroborates this comparison; a flatting of the slope of the $1/C$ curve is observed at larger thickness[11,33] as well as an increase of the slope.[12,32] Hence, no further conclusions on the influence of the different parameters used in different experiments seem reasonable.

Figure 3 summarizes the dielectric loss of the films. There is no systematic trend with small deviations from stoichiometry. However, a systematic increase with film thickness; for thickness below ~60 nm the values are well below 0.01 and for larger thickness there is a larger scatter of the values along with larger values above 100 nm thickness.

For many applications the field and temperature dependence of the dielectric constant has to be considered and some examples of complete *C-V* curves are shown in Figs. 4(a) and 4(b). The zero bias permittivity is much higher for

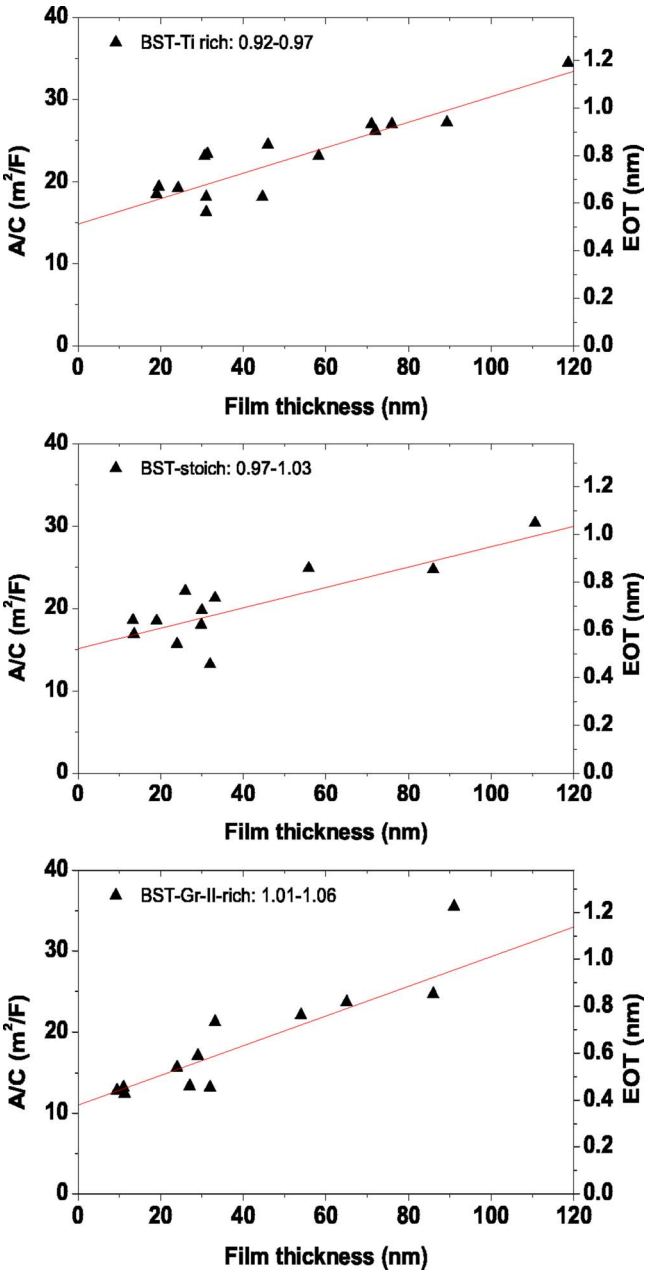

FIG. 2. Thickness dependence of the reciprocal capacitance for BST films with different Gr-II/Ti ratio.

BST than for STO, however, the field dependence is also much stronger. This behavior is quantified by the tunability of the DK,

$$\text{tunability}(V) = \frac{\varepsilon(0) - \varepsilon(V)}{\varepsilon(0)}. \tag{3}$$

For the given example of ~60 nm thick films, we obtain a value of 26% for STO and of 57% for BST at a bias voltage of 5 V. This tunability depends on the film thickness as well on the temperature, Fig. 4(b). These dependencies have been discussed in detail[24] and we will discuss here only some conclusions on the dead layer.

The demonstration of the applicability of the simple two-capacitor model is not sufficient for a proof of the underlying physics as discussed earlier.[24,30] In addition the offset yields

TABLE I. Stoichiometry dependence of dielectric properties of films deposited at $T \sim 600$ °C.

Film	Gr-II/Ti	$\varepsilon_i/2t_i$ (nm^{-1})	EOT_i (nm)	ε_B	$EOT_{20\ nm}$ (nm)	ε_{eff} at 20 nm	ε_{eff} at 60 nm
$(Ba_{0.7}Sr_{0.3})TiO_3$	0.92–0.97	7.6±2	0.51	725±30	0.62	126	281
	0.97–1.03	7.5±2	0.52	900±30	0.61	128	410
	1.01–1.06	10.3±3	0.38	620±20	0.51	154	308
$SrTiO_3$	0.94–1.05	17±3	0.23	210±20	0.60	130	174
BST-STO	0.92–0.99	8.7±3	0.45	440	0.62	124	238
STO-BST	0.92–0.99	11±2	0.35	510±50	0.51	154	288
STO-BST-STO	0.95–1.0	11±2	0.35	580	0.49	159	308

only the combined value of $\varepsilon_i/2t_i$ and a separation would be helpful for the discrimination between different models, e.g., the assumption of an electric field penetration into the metal[34] yields much smaller thickness than surface induced changes of the polarizability.[35] These approaches have been reviewed recently.[36,37] Although the field dependence has been discussed,[14] it seems that the field dependence (tunability) has not been considered so far to estimate the dead layer thickness. The tunability [Fig. 4(a)] shows a thickness independent ε at high fields, >600 kV/cm, $\varepsilon \sim 100$, i.e., there is no longer a dead layer observed. As the effective ε is still at a level of ~100, this might be considered as the lower limit for ε_i. This rather high value yields a thickness of the dead layer, $2t_i \sim 10$ nm for best BST films. Hence, structural or extrinsic defects at the interface can be excluded, as these would be visible in high-resolution transmission electron microscopy for such large thickness. As this dead layer thickness is close to the total film thickness for the thinnest films, the approximation of the two-capacitor model ($t_i \ll t$) breaks down. Such a thick layer seems best consistent with the phonon model,[35] i.e., the damping of the soft phonons in the thin film; there has been evidence for the damping from far-infrared ellipsometry,[38] however, these results are restricted to a rather thick film and the thickness dependence would be necessary for definite conclusions. On the other hand, we would expect a rather thickness independent value of ε by further reducing the thickness below 15 nm; unfortunately these thinner films were leaky, probably related to the roughness of the Pt electrodes.

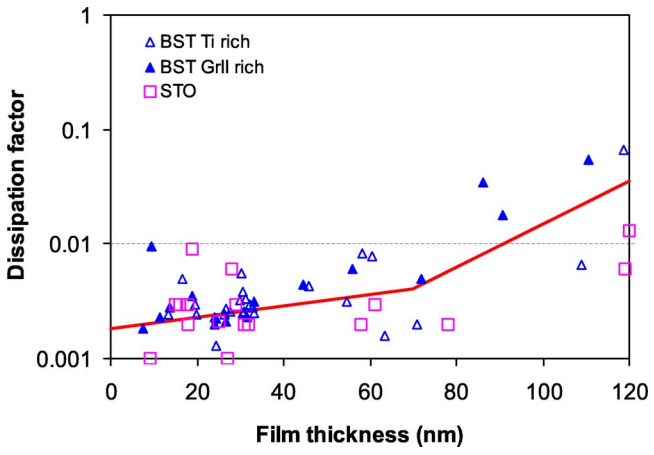

FIG. 3. Dissipation factor, tan δ, for films of different thickness.

B. Interface modulation

In order to improve the interfacial capacity different capacitor stacks were deposited with a 2 nm thick STO layer at the interface, as indicated in Fig. 5. In addition a stack with a group-II rich interlayer was produced, Gr-II-BST-Gr-II. As expected from the data of Table I these modifications show the same tendency as the STO-BST-STO films, however, the STO seems slightly better and we concentrated therefore on these modifications. Although these stacks are more complicated, in principle a five-layer stack, the simple reciprocal plot is applied in the first approximation, as shown in Fig. 5. We observe an approximate linear behavior for the different stacks. There is an indication that the bottom electrode is more important than the top electrode. The results for effective interface and bulk capacity are given in Table I as compared to the homogeneous layers. Especially for thin films,

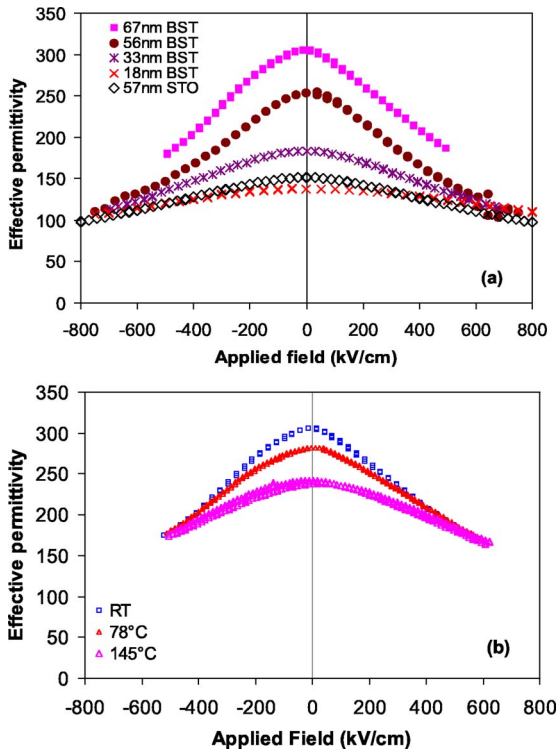

FIG. 4. (a) C-V characteristics for 15–67 nm thick BST films and of a 60 nm thick STO film. (b) Temperature dependence of the permittivity for the 67 nm thick BST film.

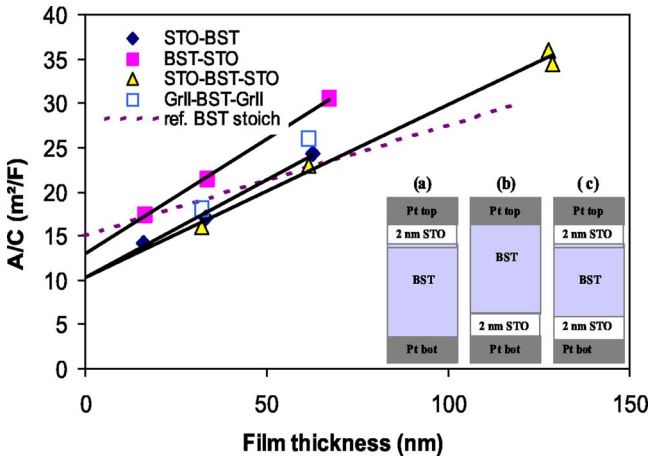

FIG. 5. Reciprocal capacitance vs film thickness for films with different interfacial layers. Inset shows the schematics of the different capacitor stacks: (a) BST-STO, (b) STO-BST, and (c) STO-BST-STO. In addition a stack with Gr-II enrichment at the interface, Gr-II-BST-Gr-II, is shown.

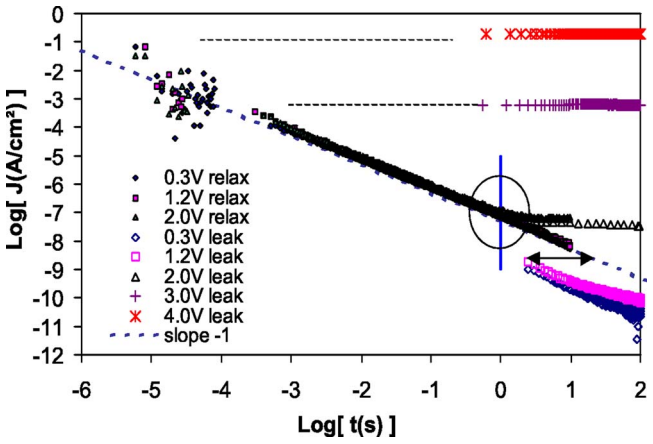

FIG. 6. Leakage current vs time curves at different applied voltages for the example of a 30 nm thick film. The different time ranges are covered by measurements in the relaxation and leakage mode, respectively. The arrow indicates a difference between the two modes, which is relevant for low voltages. The leakage current is given starting from the time of the approach of the final voltage, however, the film is under stepwise increasing bias for a much longer time and the observed value is below the universal relaxation curve. This difference corresponds to the effective time shift indicated by the arrow.

where the interface is dominant, better average values are obtained as for stoichiometric BST. However, these values are close to those for the Gr-II rich films.

IV. RELAXATION CURRENTS IN BST FILMS

For short times after a voltage step the current response of a film is controlled by the dielectric relaxation current and the stationary leakage current is obtained only after some time. Figure 6 shows the characteristic behavior over a time scale from 1 μs to 100 s. There were some problems at the transition between the different amplifiers, however, for larger times the data were quite stable. For low fields we observe a steady decay over many orders of magnitude. A similar behavior is observed for the depolarization current after switching the field off (not shown). For higher fields the turn over to the stable leakage regime is seen. The behavior of the relaxation current is well described by the Curie–von Schweidler relaxation,[39–41] which can be understood by a superposition of single relaxation processes with a very broad distribution of activation energies.

$$J(t) = J_0 t^{-n}. \tag{4}$$

The exponent n is generally $\leqslant 1$ and a slope of ~ 1 gives a good approximation for our data. As the relaxation is connected by a Fourier transformation to the frequency dependence of the dielectric constant [$\varepsilon(\omega) \sim \omega^{(n-1)}$ (Refs. 41 and 42)] values of $n > 0.995$ correspond to a dispersion of less than 0.5% per decade observed for these films. The prefactor J_0 is in the range of $(8 \pm 2) \times 10^{-8}$ A/cm^2. We observe no change with the applied field (or voltage). There is also no significant change with temperature between 23 and 150 °C, which is in agreement with earlier observations.[43] In addition we observe no dependency on the film stoichiometry. Most remarkable is, however, the observation of the independence on the film thickness (absolute value, J_0, as well as slope, n), which is similar to the high field results of Ref. 43. The thickness independence of the slope corresponds well to the independence of the loss angle, Fig. 3, as these are directly related, $\tan \delta \sim \cot(n\pi/2)$;[42,44] the small changes expected for the thickest films are, however, within the errors of these measurements. These observations indicate that the dominating dielectric relaxation of the thin films must be attributed to the interfacial layers[45,46] and not to bulk effects.[11,43,47] The total polarization can be simply integrated assuming $n=1$,

$$Q = \int J(t)dt = J_0 \ln(t). \tag{5}$$

Hence, the integral from 10^{-6} to 1 s yields 1.1 μC/cm^2 corresponding to 0.7×10^{13} e/cm^2, which amounts to about 10% of the total load of the capacitor (e.g., $C \sim 50$ fF/μm^2) at 2 V. These large relaxations at the interface might influence the modeling of the leakage currents by a possible change of the effective work function of the metal but as these processes are rather slow they should not affect the measurements of the dielectric dead layer, which are performed at 100 kHz.

In addition, Fig. 6 shows that for high fields the leakage currents are high enough to be dominating after times of ~ 10 s, whereas for low fields there is no stabilization after 10 s; for the detection of a leakage current of 10^{-11} A/cm^2 Fig. 6 indicates that a waiting time of 1000 s would be necessary. This problem is largely reduced by the stepwise increase of the voltage in the I-V curves for the leakage determination, i.e., the total measuring time is at least partly available for the relaxation as indicated by the arrow. For small voltages the leakage current is low and the relaxation is still visible, however, the absolute values are reduced. At high voltages the leakage currents are dominating from the beginning and even at 4 V (fields of 1200 kV/cm) the leakage current is stable and there is no indication of degradation of the films. Nevertheless, small degradation effects might be hidden under these high currents, and for some films a small increase of the current is observed at medium voltages, which indicate some modification under current stress. In contrast to the short time relaxation, Fig. 6, the relaxations,

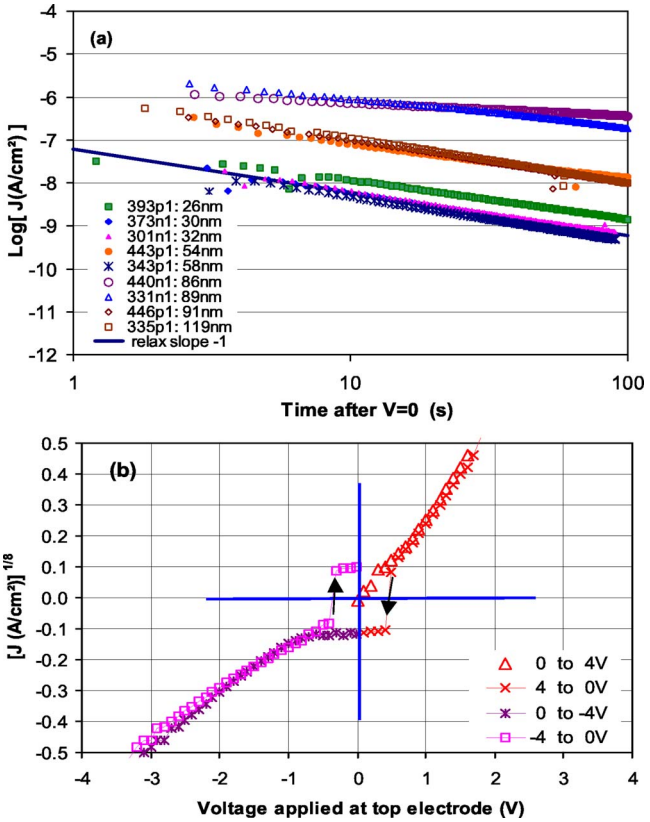

FIG. 7. (a) Depolarization currents after the maximum voltage of the leakage current measurement. (b) *I-V* loop for leakage current measurements; reverse currents are observed in the depolarization runs. Ordinate scale is changed from the logarithmic scale in part (a) in order to allow for the demonstration of the change of sign.

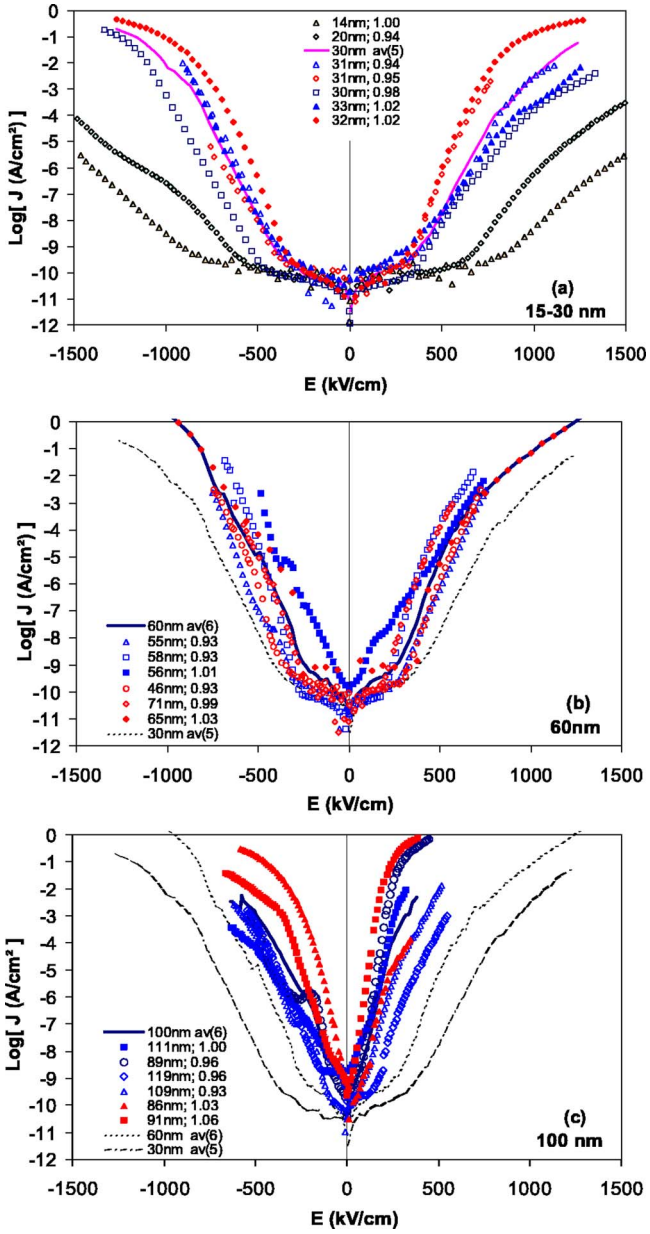

FIG. 8. Field dependence of the leakage current for BST films of different stoichiometry and different thickness. The sign of the field refers to the voltage applied to the top electrode. The average curves present the average of the logarithmic data and the number indicates the number of different measurements, which have been considered.

observed after long time current stress, Fig. 7(a), seem to be more bulk related. This becomes evident from the depolarization observed after a complete leakage current run to the maximum voltage (waiting time 100 s/step), Fig. 7(a). The thin films are still lying on the line from Fig. 6, but for thick films the relaxation currents are appreciably higher. This indicates an additional bulk effect in the polarization. Additional features of this relaxation processes are shown in Fig. 7(b), which shows a loop of the leakage measurements. We start with increasing to the maximum positive voltage; going back we observe a zero crossing at positive voltages, i.e., a reverse depolarization current, which overruns the direct leakage current. A similar behavior is observed for negative voltages. This behavior indicates the built-up of electrochemical potentials during current stress at higher voltages.

V. LEAKAGE CURRENTS IN STO AND BST FILMS

A. Room temperature leakage mechanisms in $(Ba_{0.7}Sr_{0.3})TiO_3$ thin films

The field dependence of the leakage currents is also seriously affected by the film thickness as shown if Figs. 8(a)–8(c) for BST of different thickness. Instead of a universal curve we observe a steady increase of the leakage currents with film thickness, which seems rather independent of the film stoichiometry. The leakage currents for positive and negative bias are measured on different pads in order to avoid possible degradation effects and the asymmetry of the two branches might therefore reflect the difference from pad to pad rather than a systematic difference between top and bottom electrodes. In spite of the scatter of the data there is an indication for a reproducible asymmetry for the thickest films (~100 nm), and this behavior could be reproduced with some examples for complete loops on one pad. The surface topology and rms roughness of the thinner films is mainly determined by the roughness of the Pt electrode and a significant increase in roughness is observed only for films thicker than ~60 nm, hence, the difference in the leakage behavior of the thickest films might be related to the increased roughness of the films,[20] i.e., the thinner films are quite well conformal covering the Pt structure and only for

the thicker films the grain structure of the BST films themselves becomes dominant. Remarkably, the higher currents are observed for electron injection from the bottom electrode and the roughness of the electrode structure becomes important as soon as there is no longer a conformal coverage. As the currents on the high current branch are connected with some degradation effects visible at medium voltages as discussed in Sec. IV, we will mainly consider the lower current side in the following discussion for these thick films. More detailed investigations seem necessary for a thorough discussion of the asymmetry.

The leakage currents, which are averages over the two branches, are summarized in Fig. 9(a) in the form of Schottky plots. A textbooklike Schottky behavior is shown as the reference line,

$$J = A^* T^2 \exp\left[-\frac{e_0}{kT}\left(\Phi_B - \sqrt{\frac{e_0 E}{4\pi\varepsilon_0 \varepsilon_{\mathrm{opt}}}} \right) \right], \tag{6}$$

where A^* is the effective Richardson constant, k is the Boltzmann constant, and Φ_B is the barrier height. (The slope corresponds to $\varepsilon_{\mathrm{opt}} \sim 6$, and the offset corresponds to $\Phi_B \sim 1.15$ eV if the value of the Richardson constant for free electron emission, 120 A cm^{-2} K^{-2}, is used.) However, even neglecting the thickness dependence, the individual curves show no straight line. At low fields we observe a rather slow increase, which might be fit by a Schottky behavior. However, the temperature dependence discussed below is inconsistent with this model. At medium fields we observe for all films a steep slope, which yields the well known unphysically low values for the optical dielectric constant ($\varepsilon_{\mathrm{opt}} < 1$).[10,16] Remarkably, the curves show all a similar slope, however, the onset of the steep region changes dramatically with thickness.

For further discussion the data for the leakage currents are shown in Fig. 9(b) in a double log plot. Plotting the current versus field does not change the qualitative behavior, a uniform slope and a strong shift with thickness; plotting against the applied voltage apparently reduces these shift, however, there is no obvious explanation for a voltage controlled process as discussed for amorphous oxides.[17] The most reasonable variable seems to be the internal field[11] in terms of the dielectric displacement D, which is nearly equal to the polarization P, for high-ε materials: $D = \varepsilon_0 \varepsilon E \sim P$. We have used the measured value of $\varepsilon_{\mathrm{eff}}$ at zero bias [instead of the integral $\int \varepsilon(E) dE$] in this approximation. We observe a rather universal curve for the films up to the largest thickness with a very small slope at low fields. For higher fields we observe a rather sharp change to a very steep slope. This yields a universal description of the leakage currents by

$$J(D) = J_1 D^m, \tag{7}$$

where J_1 is the current at the dielectric displacement of 1 μC/cm^2 with a value of $10^{-(21\pm1)}$ A/cm^2, and the slope m has values of $-(16\pm2)$. We restrict here to this approximation; however, an additional consideration of the field dependence of ε would further increase this slope, especially for the thicker films.

The low currents predicted from the power law at low fields cannot be observed due to the overlap with other leakage mechanisms. As discussed above, the relaxation currents dominate these currents and the increase with thickness can be attributed to the increase of these currents under current stress. Hence it is rather the level of these currents, which limits the range for the application of the power law. This transition corresponds also to applied voltages below ~1 V and the small remaining slope is close to 1; therefore this region has previously also been attributed to an Ohmic behavior.[48] Although we see that the relaxation is dominating it seems remarkable that the apparent specific resistivity is $\sim 10^{16}$ Ω cm for films ≤30 nm and reaches values of 10^{13} Ω cm for 120 nm thick films, which are all well above the values for bulk ceramics of 10^{10} Ω cm.[49] Finally, there is an indication for additional effects in the transition region for thick films, which might be attributed to the increasing roughness and corresponding influence of field inhomogeneities.

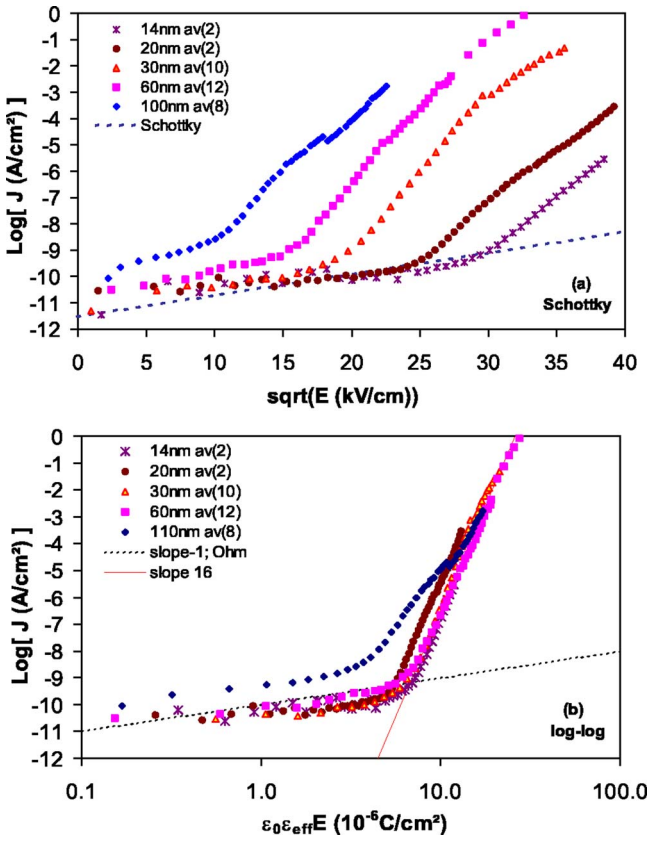

FIG. 9. (a) Schottky plot of the field dependence of the leakage current for BST films of different thickness. The logarithmic average of a number of different measurements, as given in the inset, is shown. A textbooklike Schottky behavior is indicated by a dashed line as obtained for $\varepsilon_{\mathrm{opt}}=6$ and $\Phi_B=1.1$ eV. (b) Log-log plot of the leakage current vs the dielectric displacement or polarization ($D=\varepsilon_0\varepsilon_{\mathrm{eff}}E \sim P$) for BST films of different thickness.

Hence, the leakage currents observed at RT are dominated by mechanisms, which are not easily accessible to a quantitative modeling. Even after long holding times relaxation currents dominate the leakage at low fields and other current contributions are hidden and become visible only at higher temperatures as discussed below. At high fields, corresponding to applied voltages of typically ≥1 V, we observe a very steep increase of the current with applied field.

The apparent thickness dependence can be removed by scaling with the dielectric displacement, i.e., the change of the permittivity with film thickness seems to be the underlying process. This scaling with D, which is a steady function at the interface, indicates the dominant role of the internal fields in the dielectric. Although this simple relation might be implicitly contained in model calculations for the leakage currents, which consider space charges and the details of the interfaces,[9,10,14] such a relation has not been revealed so far. Models for field injection might yield such steep slopes due to the exponential field dependence, however, using parameters, which are considered reasonable at present, less steep slopes have been reported for the region of fields considered here, and there is only a qualitative agreement with recent modeling for a 82 nm thick BST film.[9]

Additionally we observe some relaxations under current stress, which restrict the applicability as integrated capacitors,[50] and a rather large scatter of the data for different films in this high field region. These latter effects might be related to the forming and switching effects observed first for amorphous oxides[17,51] and which have more recently been shown to exhibit a reproducible switching behavior for doped crystalline films.[52] The steep slope of the I-V curves might indicate an avalanche-type evolution by the electron acceleration within the strong internal field as discussed first by O'Dwyer;[53] in contrast to these calculations for a bulk behavior we observe no negative resistance region, which must be attributed to the limitation of the currents in filaments. Hence, the behavior is comparable to the effects discussed for the electron emission into vacuum, Malter effect.[54] Additional direct evidence for the formation of conducting filaments has been discussed more recently.[18,19,55,56] Unfortunately, such mechanisms do not allow a quantitative prediction of the leakage currents.

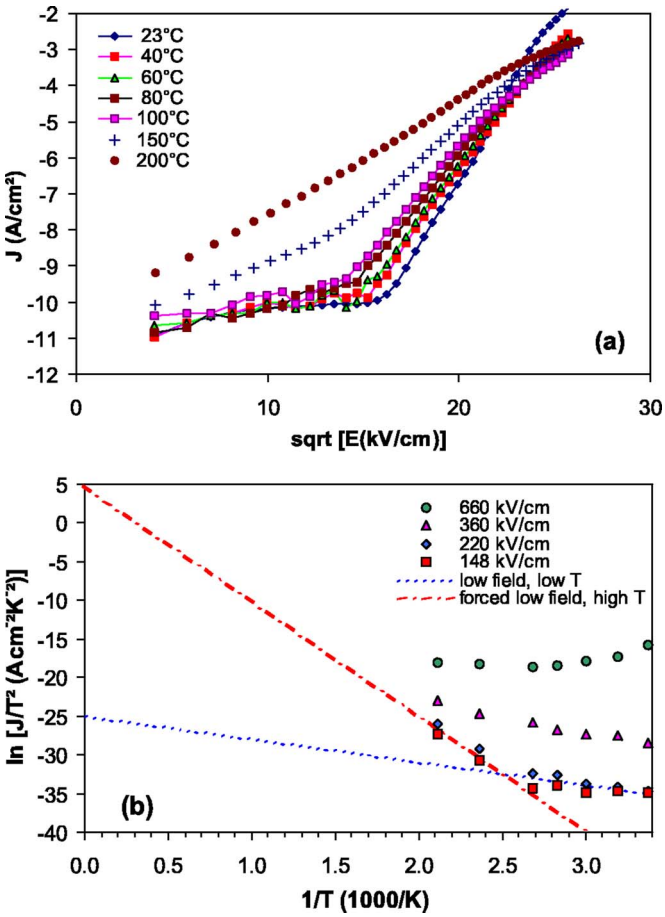

FIG. 10. Temperature dependence of the leakage current. (a) Schottky plot of the field dependence at different measuring temperatures. (b) Schottky plot of the temperature dependence at different applied fields (example for a film with 60 nm thickness). The reference line forced to value of $A^*=120$ A cm^{-2} K^{-2} at $1/T=0$ K^{-1} indicates a Schottky behavior for low fields and high temperatures.

B. Temperature dependence

Figure 10(a) shows the field dependence for different measuring temperatures for a 61 nm thick film. Up to 100 °C the behavior is very similar to the behavior at RT. We observe a small increase of the current with temperature in the low field region, a small shift of the turning point to lower fields and a corresponding higher current at medium fields, which is in agreement with earlier publications.[14,57] Finally, we observe a crossover at high fields, i.e., lower currents with increasing temperature. At temperatures above 100 °C there is a more steady transition between the two regions; especially, there is a steady increase of the current at low fields, which indicates that the currents are no longer dominated by relaxation currents. In addition we observe a further decrease of the final slope.

Figure 10(b) summarizes this temperature dependence in a Schottky plot. At low temperatures we observe a very small slope, which corresponds to an effective barrier height of 0.2–0.3 eV. At high fields the slope has even a reversed sign. Extrapolation yields values for the effective Richardson constant in the range of 10^{-7}–10^{-11}. For comparison the Schottky behavior is indicated as an additional dotted line starting at the Richardson constant of 120 A cm^{-2} K^{-2}. This slope of the line yields a reasonable value for the effective barrier height, ~1.3 eV. The rather astonishing good fit of the line to the high temperature values obtained at low fields supports the assumption that a Schottky behavior might control the leakages at temperatures above 100 °C. This overall view is further supported by the thickness dependence shown Fig. 11(a). The larger slope for the thickest film indicates additional contributions due to current stress. The data are plotted in Fig. 11(b) versus D. In this evaluation the decrease of the zero field permittivity with temperature has been considered, i.e., for a 60 nm film a reduction to ~80% of the RT value at 150 °C [Fig. 4(b)] and to ~68% at 200 °C.[24] Due to this correction the crossover of the leakage curves is removed and the leakage currents rather merge to the high field behavior. Hence, the region of positive temperature coefficient of resistance, PTCR behavior,[9,58,59] can be understood and is removed by this scaling.

Summarizing, for elevated temperatures there is a change of the dominating conduction mechanism at low fields, whereas the high field power law dependence remains valid although it is less easily reached. For the Pt electrodes considered here the low field leakage currents are dominated by relaxation currents below 100 °C and real leakage currents become dominant above 100 °C, with a transition de-

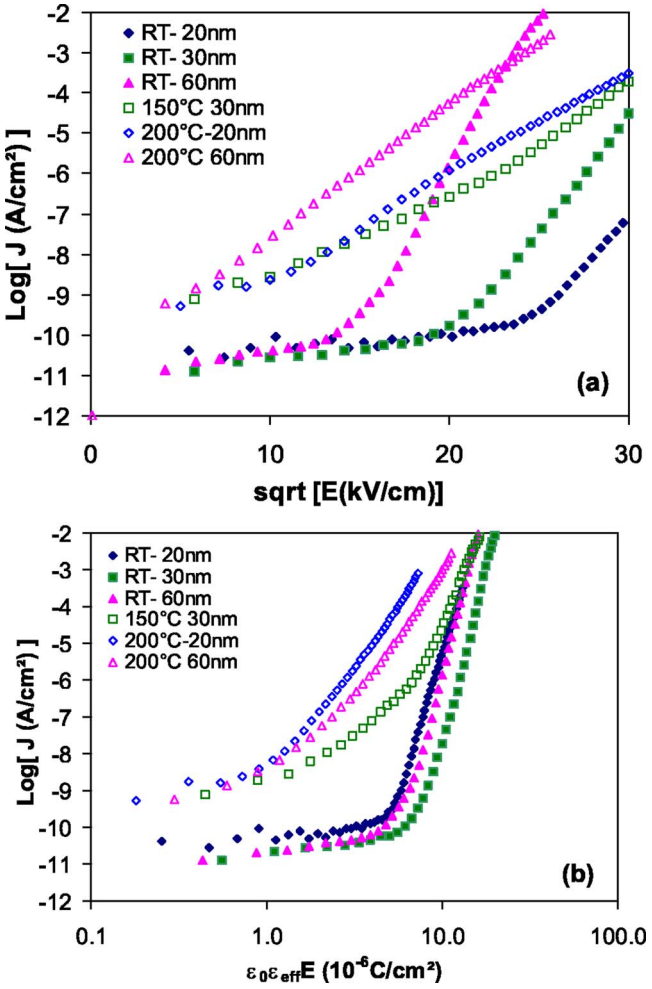

FIG. 11. Temperature and thickness dependence of the leakage current. (a) Schottky plot; (b) log-log plot of the leakage current vs dielectric displacement.

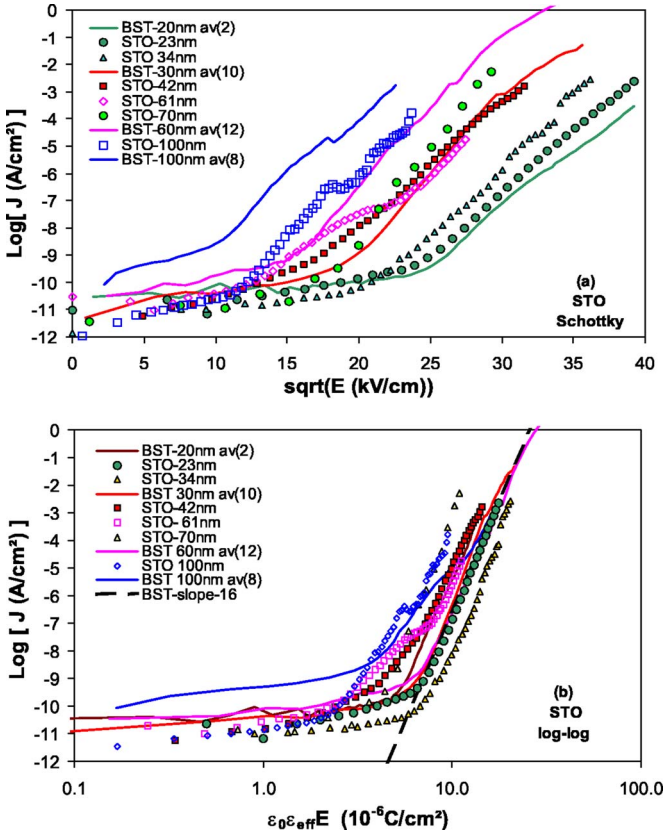

FIG. 12. Field dependence of the leakage current for STO films of different thickness. The logarithmic average of a number of different measurements, as given in the inset, is shown, and the average values for BST are included as a reference. (a) Schottky plot and (b) log-log plot of leakage current vs dielectric displacement.

fined by the magnitude of the relaxation current of $\sim 10^{-10}$ A/cm^2. For this region, $T > 100$ °C and low to medium fields, conventional leakage mechanisms dominate and the general trends shown in Figs. 10 and 11 are in qualitative agreement with the calculations.[9,10] Parenthetically, we would like to mention that for an electrode material with a lower work function these leakage mechanisms are expected to dominate at lower temperatures and much larger currents would be observed even at RT. These trends are in agreement with experimental observations of increasing leakage currents when changing from Pt to Au, Ti, and Al electrodes.[47,60]

C. Stoichiometry dependence I: STO thin films

Figure 12 shows the leakage behavior of STO films as compared to films of similar thickness of BST. In spite of the uncertainties of the individual plots, we observe a significant lower leakage for STO films. The STO curves are close to the curves for BST for the thinnest films of ~20 nm but for larger thickness the difference seems to increase. Figure 12(b) shows the data in a log-log plot versus polarization, which again essentially removes the thickness dependence. Independent of thickness there are lower currents for STO at low fields, which corresponds to somewhat lower relaxation currents; in the high field region we observe similar slopes for BST and STO, and the thin films seem to have somewhat lower leakage than BST, whereas the thicker ones are close to the thick BST films. This approach of the thicker films can be simply understood, as ε is smaller than for BST, and, consequently, also the shift by multiplication with ε.

Again, a direct comparison to published data is corroborated by the dominating thickness dependence, e.g., a comparison of a 150 nm thick STO film with a 50 nm BST film[48] cannot show the same trends. Nevertheless, a similar difference has been reported for sputter deposited 60 nm thick films of $(Ba_{0.5}Sr_{0.5})TiO_3$ and STO (Ref. 61) at a bias voltage of 3.3 V; in addition the breakdown voltages for STO films were lower than those for the BST films.

D. Stoichiometry dependence II: Gr-II/Ti ratio

The leakage currents, which have been summarized in Fig. 8, include films with different Gr-II/Ti ratios. For the ⩽30 nm thick films there is no significant difference for different Gr-II/Ti ratio within the variations, which are typically at least one order of magnitude.[60] For the thickest films of ~100 nm there are even larger variations, nevertheless, there is some indication that the group-II rich films show the highest leakage. This leakage behavior might be directly related to the higher surface roughness of these films[20] (the larger hillocks of the Ti-rich films wont hurt, but the more deep

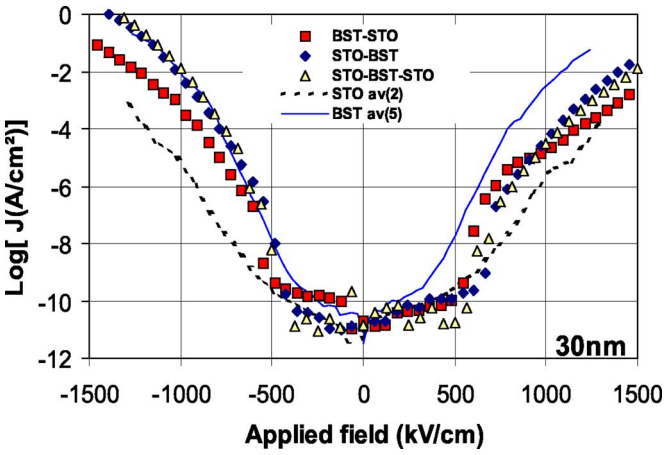

FIG. 13. Field dependence of the leakage current for BST films of 30 nm thickness and different interface structures.

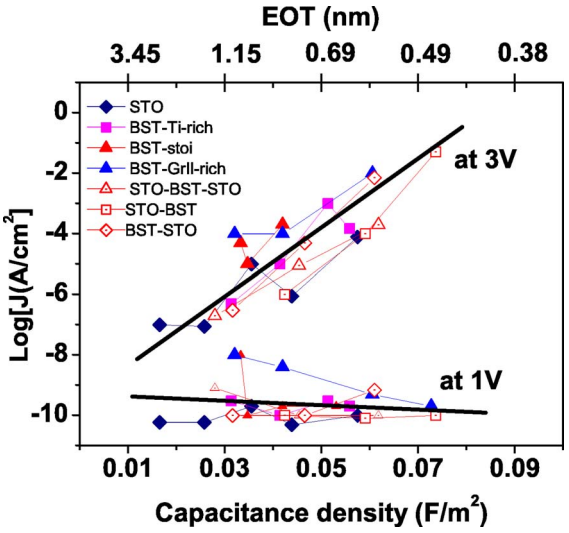

FIG. 14. Figure of merit plot for capacitors with different dielectric as given in the inset; large differences are observed at different applied voltages.

valleys at the grain boundaries of the Gr-II rich films do). Hence, these results for the thicker films reproduce earlier conclusions,[2] which reported better leakage behavior for Ti-rich films based on data from ~60 nm thick films. However, this behavior is no longer observed for the technological more relevant thin films of 15–30 nm thickness.

E. Effects of interfacial modulations

From the DK there was some indication for an improvement by interfacial modulation with STO especially for very thin films where the interfacial contribution is decisive. For a final evaluation the leakage current is important, too. Figure 13 compares the leakage behavior of the different stacks to that of BST and STO films of similar thickness. In spite of the scatter of the data we observe that the modulated films generally lie in between the reference films of BST and STO. That means that some significant improvement can be achieved as compared to pure BST films.

VI. SUMMARY AND CONCLUSION

Due to the complex interplay of bulk and interface properties the basic electrical properties, DK and leakage current, could not be scaled with film thickness in a straightforward manner. The detailed investigation the electrical properties of complete thickness series for films of different stoichiometry indicated some trends, as summarized in Table I; especially, the interfacial capacity is higher for $SrTiO_3$ films than for BST (Ba/Sr=70/30) films. Based on these data we optimized film stacks, as indicated in Fig. 5. The relative permittivity of the STO-BST and STO-BST-STO films of 30 nm thickness is very similar and similar to the behavior of BST films of the same thickness. As the leakage current is improved, too, and close to that of the STO films this small improvement is significant. In addition we have used the independence of the high field permittivity from film thickness for an estimation of the absolute thickness of the phenomenological determined dead layer; $\varepsilon/2t_i=7.5$ nm yields $2t_i=13$ nm, i.e., the thinnest films are nearly homogeneous with $\varepsilon\sim100$.

The behavior of the RT leakage current must be divided into different contributing mechanisms: for low voltages, $\leqslant 1$ V, the currents are very low, $\leqslant 10^{-10}$ A/cm^2, and dominated by the relaxation currents (Curie–von Schweidler behavior). At higher voltages a change to a very strong power law increase is observed, $J\sim E^{16}$, and the thickness dependence is removed by scaling with the internal field or polarization of the film, $D=\varepsilon_0\varepsilon E$. Hence, a direct connection between the decrease in ε and the increase in leakage with film thickness is revealed. The strong field dependence indicates an avalanche-type evolution by the electron acceleration within the strong internal field comparable to the effects discussed for the electron emission into vacuum (Malter effect). This behavior is accompanied by a larger scatter of the data and seems to be controlled by a more inhomogeneous conduction, e.g., by the formation of filaments and similarities to the resistivity switching of some oxides are indicated. The power law, as described by Eq. (7), is independent of the film stoichiometry and applies to BST as well as to STO and seems to be generally applicable to high-ε dielectrics.

These two leakage mechanisms seem to dominate for measuring temperatures from RT to ~100 °C; for higher temperatures a change is observed at low fields. The relaxation currents are buried under the increasing real leakage currents. From this reason most modeling of the leakage, which considers the Schottky barrier, has been performed for elevated temperatures,[9,10] and the general trends observed in this range of temperature and applied field (Figs. 10 and 11) are reasonably described. Nevertheless, the scaling with the dielectric displacement remains important at high fields, as the PTCR effect can be understood and is removed in this way.

Implications for the application are summarized in a figure of merit-type plot for capacitor properties, Fig. 14. These plots are quite special due to the missing scalability of DK as well as leakage and therefore change much with the voltage envisaged for the application. The highest capacity is for the individual film types obtained for the thinnest films and one simply would expect the highest leakage in this region. How-

ever, the different behavior leads to strongly different pictures. At an applied voltage of 1 V the thin films are within the relaxation-dominated region at a level of 10^{-10} A/cm^2 and there is no significant difference between all films at high capacitance. Nevertheless, there is an indication for a higher leakage for the thick Gr-II rich films. This small increase due to the increase of the relaxation currents under current stress yields the rather unusual decrease of the apparent leakage for thinner films. At a voltage of 3 V all thin films move to the region of steeper field dependence and show strongly increasing leakage for thinner films. Again Gr-II rich BST is competitive only for thin films. This correlates well with the development of the grain structure and surface roughness[20] and indicates an inhomogeneous current for these films. In summarizing, the close interrelation between the reduction of effective DK with thickness and the decrease of the leakage current yields quite different consequences: a good news for the future application at low voltages, e.g., DRAMs, as there is no increase of leakage with reduction of film thickness; a bad news for the high-ε application of thicker films as the higher DK is related to higher leakage and as there is also an increased tendency for degradation under current stress.

ACKNOWLEDGMENTS

We want to thank Dr. F. Fitsilis and Dipl. Ing. C. Christidis for the installation of the measuring systems and for performing the first measurements and Dr. S. Regnery for the deposition of most of the films. The top electrodes have been deposited and structured with the expert help of H. Haselier and D. Erdoglija. We greatly acknowledge the discussion of many different aspects of the leakage behavior with Dr. K. Szot and Dr. H. Schroeder.

[1] A. I. Kingon, J. P. Maria, and S. K. Streiffer, Nature (London) **406**, 1032 (2000).
[2] S. R. Summerfelt, in *Thin film ferroelectric materials and devices*, edited by R. Ramesh (Kluwer Academic, Boston, 1999), pp.1–42.
[3] C. S. Hwang, Mater. Sci. Eng., B **B56**, 178 (1999).
[4] M. Yoshida, H. Yabuta, S. Yamamichi, H. Yamaguchi, S. Sone, K. Iizuka, S. Nishimoto, and Y. Kato, J. Electroceram. **3**, 123 (1999).
[5] T. Horikawa *et al.*, Mater. Res. Soc. Symp. Proc. **541**, 3 (1999).
[6] M. Tarutani, M. Yamamuka, T. Takenaga, T. Kuriowa, and T. Horikawa, Thin Solid Films **409**, 8 (2002).
[7] A. I. Kingon and S. K. Streiffer, Curr. Opin. Solid State Mater. Sci. **4**, 39 (1999).
[8] J. D. Baniecki, R. B. Laibowitz, T. M. Shaw, C. Parks, J. Lian, H. Xu, and Q. Y. Ma, J. Appl. Phys. **89**, 2873 (2001).
[9] J. D. Baniecki, T. Shioga, K. Kurihara, and N. Kamehara, J. Appl. Phys. **97**, 114101 (2005).
[10] H. Schroeder and S. Schmitz, Appl. Phys. Lett. **83**, 4381 (2003); H. Schroeder, S. Schmitz, and P. Meuffels, *ibid.* **82**, 781 (2003).
[11] G. Steinlesberger, H. Reisinger, H. Bachhofer, H. Schroeder, and W. S. M. Werner, Integr. Ferroelectr. **38**, 249 (2001).
[12] D. E. Kotecki *et al.*, IBM J. Res. Dev. **43**, 367 (1999).
[13] R. Dittmann, R. Plonka, E. Vasco, N. A. Pertsev, J. Q. He, C. L. Jia, S. Hoffmann-Eifert, and R. Waser, Appl. Phys. Lett. **83**, 5011 (2003).
[14] J. C. Shin, J. Park, C. S. Hwang, and H. J. Kim, J. Appl. Phys. **86**, 506 (1999).
[15] F. Fitsilis, S. Regnery, P. Ehrhart, R. Waser, F. Schienle, M. Schumacher, and H. Juergensen, Integr. Ferroelectr. **38**, 211 (2001).
[16] J. F. Scott, *Ferroelectric Memories* (Springer, Berlin, 2000), pp. 79–120.
[17] G. Dearnaly, A. M. Stoneham, and D. V. Morgan, Rep. Prog. Phys. **33**, 1129 (1970).
[18] A. Gruverman, in *Nanoscale Phenomena in Ferroelectric Thin Films*, edited by S. Hong (Kluwer Academic, Boston, 2004), p. 57.
[19] K. Szot, W. Speier, R. Carius, U. Zastrow, and W. Beyer, Phys. Rev. Lett. **88**, 075508-1 (2002).
[20] S. Regnery, Y. Ding, P. Ehrhart, C. L. Jia, K. Szot, R. Thomas, and R. Waser, J. Appl. Phys. **98**, 084904 (2005).
[21] C. S. Kang *et al.*, Jpn. J. Appl. Phys., Part 1 **36**, 6946 (1997).
[22] C. S. Hwang, S. Y. No, J. Park, H. J. Kim, H. J. Cho, Y. K. Han, and K. Y. Oh, J. Electrochem. Soc. **149**, G585 (2002).
[23] W.-J. Lee, R. R. Woolcott, Jr., C. Basceri, H. J. Lee, S. K. Streiffer, A. I. Kingon, and D.-Y. Yang, J. Korean Phys. Soc. **32**, S1652 (1998).
[24] C. Basceri, S. K. Streiffer, A. I. Kingon, and R. Waser, J. Appl. Phys. **82**, 2497 (1997).
[25] T. Kawahara, S. Matsuno, M. Yamamuka, M. Tarutani, T. Sato, T. Horikawa, F. Uchikawa, and K. Ono, Jpn. J. Appl. Phys., Part 1 **38**, 2205 (1999).
[26] B. T. Lee and C. S. Hwang, Appl. Phys. Lett. **77**, 124 (2000).
[27] T. Horikawa, J. Tanimura, T. Kawahara, M. Yamamuka, M. Tarutani, and K. Ono, IEICE Trans. Electron. **E81-C**, 497 (1998).
[28] P. Ehrhart, F. Fitsilis, S. Regnery, R. Waser, F. Schienle, M. Schumacher, H. Juergensen, and W. Krumpen, Integr. Ferroelectr. **45**, 59 (2002).
[29] S. Regnery *et al.*, Mater. Res. Soc. Symp. Proc. **748**, U15.6.1 (2003).
[30] S. K. Streiffer, C. Basceri, C. B. Parker, S. E. Lash, and A. I. Kingon, J. Appl. Phys. **86**, 4565 (1999).
[31] T. Kawahara, M. Yamamuka, A. Yuuki, and K. Ono, Jpn. J. Appl. Phys., Part 1 **34**, 5077 (1995).
[32] W.-J. Lee, H.-G. Kim, and S.-G. Yoon, J. Appl. Phys. **80**, 5891 (1996).
[33] H. J. Cho and H. J. Kim, J. Electrochem. Soc. **145**, 3884 (1998).
[34] C. T. Black and J. J. Welser, IEEE Trans. Electron Devices **46**, 776 (1999).
[35] C. Zhou and D. M. Newns, J. Appl. Phys. **82**, 3081 (1997).
[36] L. J. Sinnamon, R. M. Bowman, and J. M. Gregg, Appl. Phys. Lett. **78**, 1724 (2001).
[37] L. J. Sinnamon, J. McAneney, R. M. Bowman, and J. M. Gregg, J. Appl. Phys. **93**, 736 (2003).
[38] A. A. Sirenko, C. Bernard, A. Golnik, A. M. Clark, J. Hao, W. Si, and X. X. Xi, Nature (London) **404**, 373 (2000).
[39] J. Curie, Ann. Chim. Phys. **18**, 203 (1889).
[40] E. von Schweidler, Ann. Phys. **24**, 711 (1907).
[41] A. K. Jonscher, *Dielectric Relaxation in Solids* (Chelsea Dielectric, London, 1983).
[42] S. K. Streiffer, C. Basceri, A. I. Kingon, S. Lipa, S. Bilodeau, R. Carl, and C. P. Van Buskirk, Mater. Res. Soc. Symp. Proc. **415**, 219 (1996).
[43] M. Schumacher and R. Waser, Integr. Ferroelectr. **22**, 109 (1998).
[44] J. D. Baniecki, R. B. Laibowitz, T. M. Shaw, P. R. Duncombe, D. A. Neumayer, D. E. Kotecki, H. Shen, and Q. Y. Ma, J. Appl. Phys. **72**, 498 (1998).
[45] J.-H. Ahn, W.-J. Lee, and H.-G. Kim, Jpn. J. Appl. Phys., Part 1 **37**, 6472 (1998).
[46] Y. Fukuda, K. Numata, K. Aoki, and A. Nishimura, Jpn. J. Appl. Phys., Part 1 **35**, 5178 (1996).
[47] R. Waser, in *Science and Technology of Electroceramic Thin Films*, NATO Advanced Studies Institute, Series E: Applied Science edited by O. Auciello and R. Waser (Kluwer Academic, Boston, 1995), p. 223.
[48] G. W. Dietz, M. Schumacher, R. Waser, S. K. Streiffer, C. Basceri, and A. J. Kingon, J. Appl. Phys. **82**, 2359 (1997).
[49] U. Syamaprasad, R. K. Galgali, and B. C. Mohanty, Mater. Lett. **7**, 197 (1988).
[50] Y. Shimada *et al.*, Jpn. J. Appl. Phys., Part 1 **35**, 4919 (1996).
[51] D. P. Oxley, Electrocomponent Science and Technology **3**, 217 (1977).
[52] A. Beck, J. G. Bednorz, Ch. Gerber, C. Rossel, and D. Widmer, Appl. Phys. Lett. **77**, 139 (2000).
[53] J. J. O'Dwyer, J. Appl. Phys. **40**, 3887 (1969).
[54] L. Malter, Phys. Rev. **50**, 48 (1936).
[55] C. Rossel, G. I. Meijer, D. Bremaud, and D. Widmer, J. Appl. Phys. **903**, 2892 (2001).
[56] K. Szot, W. Speier, G. Bihlmayer, and R. Waser, Nat. Mater. . **5**, 312 (2006).
[57] K. H. Ahn, S. B. Kim, and S. Baik, J. Appl. Phys. **93**, 1725 (2003).
[58] S. Saha, D. Y. Kaufman, S. K. Streiffer, and O. Auciello, Appl. Phys. Lett. **83**, 1414 (2002).
[59] D-S. Jeong, K. H. Ahn, W. Y. Park, and C. S. Hwang, Appl. Phys. Lett. **84**, 94 (2004).
[60] H. Schroeder and S. Schmitz, Mater. Res. Soc. Symp. Proc. **748**, U6.2.1 (2003).
[61] B. A. Baumert *et al.*, Integr. Ferroelectr. **17**, 165 (1977).